Batteries & Supercaps

Research Article
doi.org/10.1002/batt.202300573

Chemistry Europe
European Chemical Societies Publishing

www.batteries-supercaps.org

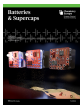

Unveiling the Potential of Silicon-Air Batteries for Low-Power Transient Electronics: Electrochemical Insights and Practical Application

Saul Said Montiel Guerrero,[a, b] Yasin Emre Durmus,*[a] Hermann Tempel,[a] Christian Roth,[c] Hans Kungl,[a] Stefan van Waasen,[b, c] Yair Ein-Eli,[d, e] and Rüdiger-A. Eichel[a, f]

With growing demand for energy storage alternatives, silicon-air batteries have gained attention due to their impressive theoretical specific energy (8470 Wh kg_{Si}^{-1}) and theoretical specific capacity (3820 mAh g_{Si}^{-1}). Although current challenges, such as corrosion, low anode mass conversion efficiency, and limited power output, restrict their practical use and commercialization potential, the ongoing advancement of materials and efficient electronic components open up a range of potential applications for Silicon-air (Si-air) batteries. This study investigates the feasibility of employing a single alkaline or non-aqueous silicon-air battery to power low-power transient electronic device. Initially, their electrochemical behavior, corrosion parameters, and performance were assessed, yielding crucial parameters for the circuit design. Short-term galvanostatic discharge experiments demonstrated the effective operation of Si-air battery under varying current densities in both electrolytes without passivation issues. Subsequently, a proof-of-concept for self-consumed and self-destructive transient electronic device is presented, wherein a full-cell Si-air battery with non-aqueous and aqueous electrolytes was operated while powering a light-emitting diode (LED) as a practical illustrative application.

Introduction

The continuously growing need for resource-efficient energy storage devices has initiated significant interest in advancing novel battery technologies.[1,2] Among these, metal-air batteries have been considered a promising development due to their high theoretical specific energies and utilization of low-cost, safe, and abundant electrode materials.[3] Specifically, Silicon-air (Si-air) batteries have received significant attention for utilizing highly resource efficient and low-cost active material.[4] More importantly, such batteries can offer remarkably high theoretical specific energy of 8470 Wh kg_{Si}^{-1} and specific capacity of 3820 mAh g_{Si}^{-1} owing to their 4-electrons transfer per Si. While Si-air batteries possess such promising advantages, their practical usage is still limited due to lack of rechargeability and the high activity of Si in both aqueous and non-aqueous media.

The development of Si-air batteries has been initiated after their first introduction in 2009.[5] The first approach to utilize highly doped Si as a fuel in a primary battery involved employing a room temperature ionic liquid (RTIL) 1-ethyl-3-methylimidazolium oligofluorohydrogenate ($EMIm(HF)_{2.3}F$), as the electrolyte. Such a novel non-aqueous Si-air battery demonstrated discharge voltages ranging from 0.8 to 1.2 V under current densities of up to 0.3 mA cm^{-2}, with discharge capacities reaching 54 mAh cm^{-2}.[6] Basing on the promising electrochemical results, further studies focused on understanding the mechanisms influencing the battery behavior under various conditions.[7–11] For example, a comparative analysis of Silicon anodes based on crystal orientation and dopant type revealed that As<111> Si anodes were considered the best choice for non-aqueous Si-air batteries due to exhibiting practical specific energies exceeding 1600 Wh kg_{Si}^{-1}.[10] However, under dynamic discharge conditions, where batteries are discharged intermittently or stored for relatively long durations, B-doped Si anodes were found to be the more favorable electrode type, providing practical specific capacities of up to 1790 mAh g_{Si}^{-1}.[11]

The aqueous Si-air batteries employing conventional potassium hydroxide (KOH) electrolytes have also been the focus of research in recent years. The initial studies have indicated the requirement of micro- or nano-porous Si surfaces to achieve

[a] S. S. Montiel Guerrero, Y. E. Durmus, H. Tempel, H. Kungl, R.-A. Eichel
Institute of Energy and Climate Research – Fundamental Electrochemistry (IEK-9), Forschungszentrum Jülich GmbH, 52428 Jülich, Germany
E-mail: y.durmus@fz-juelich.de

[b] S. S. Montiel Guerrero, S. van Waasen
University of Duisburg-Essen, Department of Electrical Engineering and Information Technology, 47057 Duisburg, Germany

[c] C. Roth, S. van Waasen
Central Institute of Engineering, Electronics and Analytics – Electronic Systems (ZEA-2) Forschungszentrum Jülich GmbH, 52428 Jülich, Germany

[d] Y. Ein-Eli
Grand Technion Energy Program, Technion – Israel Institute of Technology, Haifa 3200003, Israel

[e] Y. Ein-Eli
Department of Materials Science and Engineering, Technion – Israel Institute of Technology, Haifa 3200003, Israel

[f] R.-A. Eichel
Institut für Materialien und Prozesse für elektrochemische Energiespeicher- und wandler, RWTH Aachen University, 52074 Aachen, Germany

Supporting information for this article is available on the WWW under https://doi.org/10.1002/batt.202300573

prolonged discharge durations of up to 30 h under 0.05 mA cm^{-2}.[12,13] Otherwise, without such surface modifications, cell voltage rapidly decays when subjected to currents due to passivation of the Si surface within seconds. Subsequent research, on the other hand, reported extended discharge durations up to 270 h under 0.05 mA cm^{-2} with a refill-type cell setup while utilizing a Si anode with an unmodified surface.[14] When a thicker Si wafer (3 mm) was employed as an anode electrode, the alkaline Si-air battery (with 5 M KOH electrolyte) could be operated up to 1100 h at voltages above 1.1 V, resulting in specific capacities of 115 mAh g_{Si}^{-1} and anode mass conversion efficiencies of ~3%.[14] By lowering the KOH concentration to 0.5 M, recent research achieved enhanced Si anode utilization during discharge, exhibiting conversion efficiencies reaching up to 9%.[15] The significance of silicate concentration within the electrolyte has also been highlighted, as critical concentrations may lead to the passivation of the Si surface. The reason for achieving only a small percentage of the theoretical specific capacity (3820 mAh g_{Si}^{-1}) in the experiments can be attributed to the high activity of Si anode in the concentrated alkaline electrolytes,[16–20] which results in high corrosion rates that consume the active material and remain as the main challenge for high performing alkaline Si-air batteries. Potential strategies to address this issue involve the utilization of electrolyte additives that function as corrosion inhibitors or modification of silicon surfaces by metal-organic segments.[21] In a recent study, the favorable impact of polyethylene glycol (PEG) on the corrosion characteristics of alkaline Si-air batteries has been reported, resulting in a noteworthy enhancement of conversion efficiencies by as much as 13%.[22]

Until now, although several types of metal-based transient batteries have been reported, the use of metal-air batteries within a transient electronics concept has not been considered, possibly due to the complexity of the battery systems.[23,24] To promote the development of transient electronics using transient batteries, it is crucial to broaden the scope of material research beyond conventional battery materials. Therefore, in this study, we exploit the electrochemical reactions and the corrosion of Si within a low-power transient electronic device to function as a hardware secure system. Hardware secure systems are one line of development within the emerging field of transient electronics, which are specifically engineered for operation over a predetermined lifecycle, followed by self-disintegration upon cessation of this period or in response to a designated trigger signal, as elucidated by Hwang et al.[25] and Jam et al..[26] The concept of "on-demand hardware destruction" offers an alternative approach to the conventional practice of software-based encryption, facilitating the deactivation of the electronic device upon completion of its intended use or safeguarding sensitive information residing within the semiconductor chips, as explored in studies by Chen et al.[27] and Lee et al..[28]

Approaches to design such devices suitable to destroy the silicon components therein make use of thermal, mechanical, chemical, and electro-chemo-mechanical mechanisms. Heat-triggered thermal expansion mismatch induced by high thermal expansion material filled in grooves on the back of Si-chips leads to their destruction owing to crack formation and propagation.[29] Devices integrating gelled CuO/Al nano-thermite films that directly apply the impact of heat via melting the surfaces of the silicon components were successfully designed and tested.[30] Proof of concept for a hardware secure device employing chemical dissolution of silicon was provided by the integration of a microfluidic reservoir. In an alternative approach for a microfluidic system to dissolve electronic components on demand, KOH or sodium hydroxide (NaOH) were utilized as etchants.[28] Electrochemically induced destruction of silicon membranes by means of intercalation of Lithium was also demonstrated.[27] The Lithium intercalation leads to the chemical poisoning of silicon devices as well as to their mechanical destruction via the large volume expansion on the formation of the Li_xSi alloy. The most recent design combines the impact of melting Lithium to form Li_xSi, resulting in crack initiation with subsequent application of fluids to achieve complete destruction of the Si circuit .[31]

The present work aims to develop a design for a hardware secure device, in which the electrolyte used for running the battery power supply of the device is used for dissolving the silicon circuit components after terminating the operation. In order to match the battery parameters required for the operation of the device, the electrochemical behavior and performance characteristics of the 2 classes, namely of non-aqueous and aqueous Si-air batteries, were evaluated to acquire the essential parameters for the electronic circuit design. Subsequently, a proof-of-concept for transient electronic devices *via* a self-consumption process is now being presented for the first time, wherein the above 2 classes of Si-air batteries are operated and self-consumed, while powering a LED, as an illustrative application. Alongside the assessment of the performance of the batteries, the state and condition of the printed circuit board (PCB) and circuit elements are evaluated and reported after the batteries end of operational life.

Results and Discussion

Si-air battery based on aqueous alkaline electrolyte: Figure 1a represents the open-circuit voltage (OCV) profile of Si-air battery utilizing a 5 M KOH (alkaline) electrolyte. The OCV of the alkaline battery initiates at approximately 1.43 V and remains relatively stable over a 24 h period. Such a stable profile indicates that the Silicon surface remains active under the given OCV conditions.

Figure 1b shows the potentiodynamic polarization curves of the Silicon anode and the air cathode in alkaline media. The Silicon anode exhibits a corrosion potential of −1.37 V vs. Hg/HgO and it demonstrates a typical passivation behavior when subjected to large anodic polarizations as the current eventually drops below 0.01 mA cm^{-2}.[32] The passivation peak occurs at −1.0 V vs. Hg/HgO with a current density of 0.1 mA cm^{-2}. In comparison to Silicon, the air cathode is capable of delivering significantly higher current densities (>1 mA cm^{-2}) during polarization.

Research Article
doi.org/10.1002/batt.202300573
Chemistry Europe
European Chemical Societies Publishing

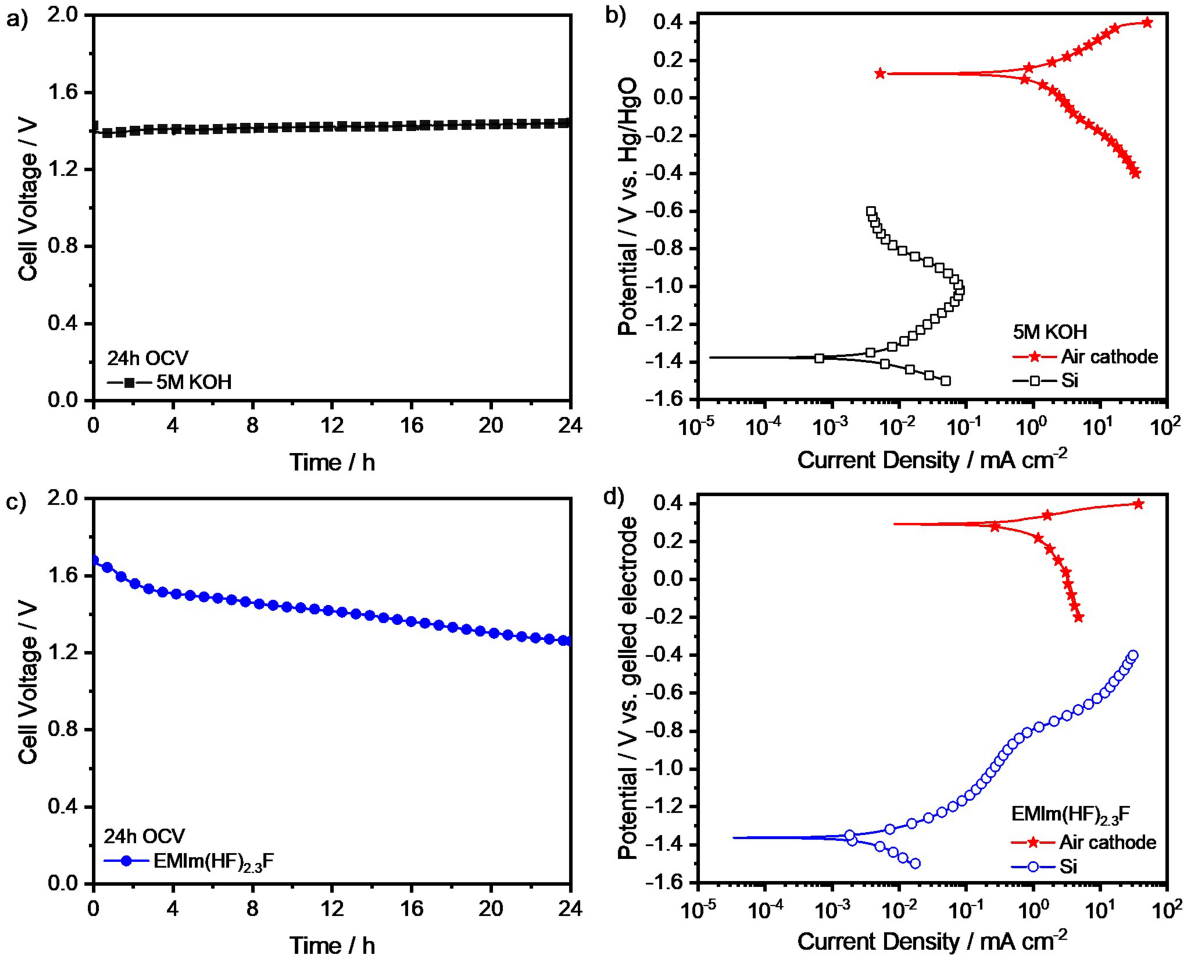

Figure 1. a) OCV profile of the alkaline Si-air battery, b) potentiodynamic polarization curves of Si anode and air cathode in 5 M KOH, c) OCV profile of the non-aqueous Si-air battery, d) potentiodynamic polarization curves of Si anode and air cathode in $EMIm(HF)_{2.3}F$. The scan rate was 5 mV s^{-1}.

Additionally, the corrosion current density of 4.9 μA cm^{-2} (corresponding to a corrosion rate of 5.5 nm h^{-1}) is obtained from the polarization curve of the Si anode. It is important to note that the corrosion currents obtained from the potentiodynamic polarization experiments solely consider electrochemical reactions, excluding chemical corrosion rates. The corrosion rates calculated using this method may differ by several orders of magnitude from the actual corrosion rates, especially in the case of Si.[20,33]

Based on the potentiodynamic polarization curves depicted in Figure 1b, it is evident that the Si-air battery can effectively be operated at current densities below 0.1 mA cm^{-2}, while maintaining discharge voltages around 1.2 V. The Silicon anode imposes limitations on the achievable current densities due to the surface passivation phenomena. The limitation arises from the accumulation of discharge products, which leads to the passivation of the Si surface as a result of local concentration gradients at high anodic potentials. The degree of the passivation phenomena in relation to the anodic potentials have previously been reported by cyclic voltammetry experiments.[14,33–35] When evaluating the suitability of employing Si-air battery in practical applications, it is crucial to consider these aspects, particularly in terms of the desired voltage and current requirements within specific applications.

Si-air battery based on non-aqueous $EMIm(HF)_{2.3}F$ electrolyte: When compared to the alkaline Si-air battery, the battery employing $EMIm(HF)_{2.3}F$ (non-aqueous) electrolyte exhibits a higher initial OCV at 1.60 V, as shown in Figure 1c. However, the voltage of the non-aqueous Si-air battery is not as constant as the one in alkaline, as it decreases to 1.26 V after 24 h. Such a decay suggests the existence of possible surface reactions at the electrodes or modification of the electrolyte content by reaction products. A similar trend has also been observed in the Ti-air battery (with $EMIm(HF)_{2.3}F$), with its OCV exhibiting a decay of 400 mV over a period of 180 h.[36] Despite the observed decay in OCV, both Si- and Ti-air batteries can still be discharged with current densities of up to 0.5 mA cm^{-2}.[10,36]

Figure 1d presents the potentiodynamic polarization curves of both silicon and air electrodes immersed in a non-aqueous electrolyte. Similar to the alkaline media, the air electrode is capable of delivering current densities >1 mA cm^{-2} at low overpotentials. The Silicon electrode exhibits a corrosion potential of -1.36 V vs. Cp_2Fe/Cp_2F^+ based reference electrode

Research Article
doi.org/10.1002/batt.202300573
Chemistry Europe
European Chemical Societies Publishing

and a corrosion current of 2.7 $\mu A\,cm^{-2}$ (corresponding to a corrosion rate of 0.04 $nm\,min^{-1}$).

Unlike the alkaline system, the Si electrode does not show a passivation behavior even under significant anodic polarizations. The electrode can achieve current densities of up to 1 $mA\,cm^{-2}$ at anodic overpotentials of 0.5–0.6 V. However, it is worth mentioning that such high anodic overpotentials may lead to the formation of a surface layer which is possibly composed of silicon-fluoride (Si–F) elements. This surface layer, which facilitates ion transfer, does not show significant resistive behavior, as the oxidation of Si can still take place. Similar surface layer formations have also been reported for the aluminum (Al) and titanium (Ti) metals upon exposure of $EMIm(HF)_{2.3}F$[36,37] or tetra-butyl ammonium fluoride based[38] electrolytes. Based on the polarization behavior of both electrodes, the non-aqueous Si-air battery is capable of delivering current densities up to 0.3 $mA\,cm^{-2}$ while maintaining voltages of 1.2 V. In terms of the achievable maximum current densities without passivation, there seems to be no limitation of both electrodes. However, it is important to emphasize that the discharge voltage plays a significant role in effectively powering electronic devices.

A comparison between the two Si-air battery systems: Figure 2 presents the galvanostatic discharge profiles of alkaline and non-aqueous Si-air batteries with various discharge current densities under ambient conditions. The cell voltage-capacity curves and the cell reactions are provided in the supplementary (Figure S1). The alkaline Si-air batteries exhibited a stable OCV of 1.4 V for a duration of 4 h (Figure 2a). When discharging the batteries with 0.025 and 0.05 $mA\,cm^{-2}$ current densities, the average discharge voltages of 1.34 V and 1.26 V were recorded, respectively. At a slightly higher discharge current density of 0.07 $mA\,cm^{-2}$, the average discharge voltage further decreased to 1.20 V. It is worth noting that higher discharge current densities, such as 0.1 $mA\,cm^{-2}$, led to premature discharge termination of the batteries due to the instantaneous passivation of the Silicon surface.

The non-aqueous Si-air batteries could be discharged at much higher discharge current densities as shown in Figure 2b. Following an initial OCV period of 4 h, applying a discharge current density of 0.05 $mA\,cm^{-2}$ resulted in a discharge voltage of 1.42 V. However, it decreased to 1.11 V over a duration of 20 h. Similarly, when discharging with a higher current density of 0.3 $mA\,cm^{-2}$, the battery exhibited an initial voltage of 1.16 V, which decayed by approximately 400 mV to 0.75 V after 20 h. Such a decay is mostly related to the possible surface reactions taking place at the Si/electrolyte interface, which could potentially result in the electrolyte degradation over time.[9]

Discharging the Si-air batteries revealed a significant difference in specific energies between the two electrolytes. In the case of the alkaline battery, specific energies of up to 132 $Wh\,kg_{Si}^{-1}$ could be achieved under a discharge current density of 0.07 $mA\,cm^{-2}$. On the other hand, the non-aqueous battery exhibited remarkably higher specific energies, reaching up to 1300 $Wh\,kg_{Si}^{-1}$. This nearly ten-fold difference in specific energies can be attributed to both the distinct activities and stability of the Silicon anodes in the two electrolytes and the achievable current densities.

Si demonstrates high reactivity in alkaline media, leading to (electro-)chemical dissolution through corrosion reactions at substantial rates.[16,20,33,39] For instance, in concentrated KOH solutions, corrosion rates of up to 2400 $nm\,h^{-1}$ have been observed for Si.[20,40] During the battery operation, such high corrosion rates would considerably reduce the utilized specific energies due to the consumption of active material. In comparison, Si demonstrates a milder corrosion behavior in the non-aqueous ionic liquid,[6] with corrosion rates of up to 140 $nm\,h^{-1}$.[10] The corrosion rates based on the gravimetric weight loss of Si anodes from Figure 2 is depicted in Figure S2.

Additionally, the passivation behavior of Si in alkaline media imposes limitations on the achievable current densities, as discussed in Figure 1b. Apart from the more favorable corrosion behavior, the non-passivating nature of Si in non-aqueous media also plays a role in enabling higher specific energies in non-aqueous Si-air batteries. Unlike in alkaline media where

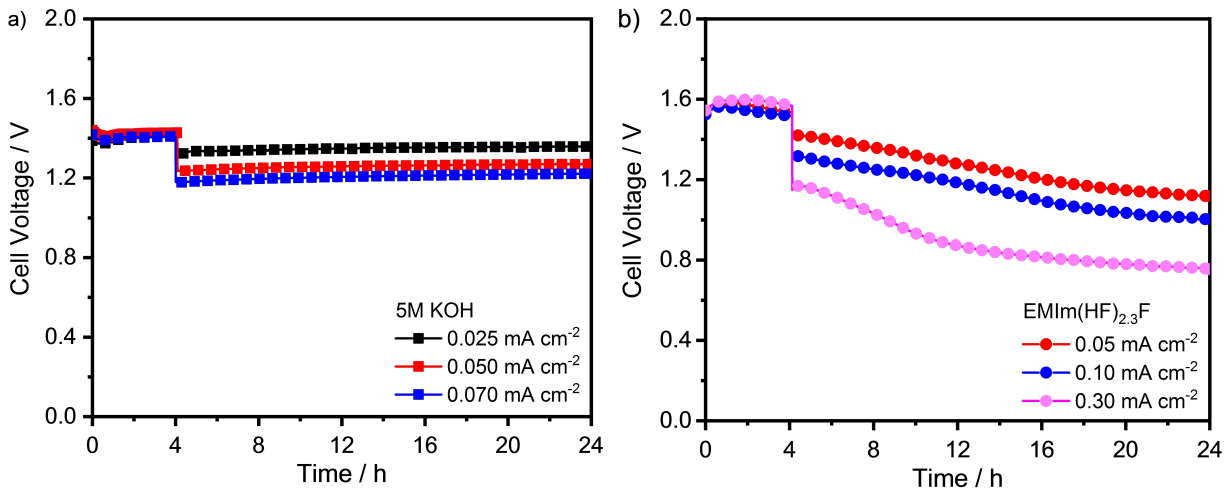

Figure 2. Galvanostatic discharge profiles of a) alkaline Si-air batteries, b) non-aqueous Si-air batteries under various current densities.

Research Article
doi.org/10.1002/batt.202300573
Chemistry Europe
European Chemical Societies Publishing

passivation occurs beyond 0.1 mA cm^{-2} current densities, the absence of passivation in non-aqueous media allows for sustained activity even at substantially higher current densities, leading to the realization of higher specific energies and better performance in non-aqueous Si-air batteries.

Vanishing Si-air battery in transient electronics

In order to have a suitable design for a transient electronic device capable of operating within a predefined time frame without the need for additional components, such as an electrolyte pump (as observed in previous experiments involving alkaline Si-air batteries), it is essential to consider following parameters: silicon thickness, active area, corrosion rate, and electrolyte volume. As the alkaline system poses the most limitations regarding to the cell requirements (passivation, electrolyte pump, current densities, silicate solubilities), mostly the challenges related to the alkaline system were considered for the transient electronic design.

Silicon anode with a thickness of 600 μm was used to be able to discharge up to around 250 h according to the etching rates obtained from Figure 2a. Based on the initial analysis of the circuit, the absolute current output of the battery was required to be around 0.140 mA. Based on previous research findings, it is established that silicon electrodes can deliver maximum current densities of approximately 0.07 mA cm^{-2}. Therefore, the active electrode area was selected to be 2.8 cm^2 in order to achieve a target current density of 0.05 mA cm^{-2}. Additionally, the electrolyte volume should be adequate to facilitate the dissolution of discharge/corrosion products without implementing any limitations on the discharge behavior. The electrolyte volume was fixed to 3.0 mL, taking into account the solubility limits of silicates (4 M) in a 5 M KOH solution.[14] The non-aqueous system was also operated using the same setup.

Prior conducting the experiments demonstrating a coupling of the PCBs with the Si-air batteries towards transient electronics, cyclic voltammetry (CV) experiments were performed using the modified battery setup from Figure 6. Figure 3a displays the CV profile of the alkaline Si-air battery, which achieved anodic current densities of up to 0.08 mA cm^{-2} at around voltages of 1.0 V. It is noteworthy that the battery exhibited no passivation characteristics even after two consecutive cycles. The non-aqueous Si-air battery demonstrated anodic current values above 0.5 mA cm^{-2} around 1 V, without displaying any passivation behavior. The pronounced difference between the two systems can also be seen from the power density curves (Figure S3).

The current densities observed at these discharge voltages in both the alkaline and non-aqueous Si-air batteries are sufficient to activate the DC/DC converter and power the LED effectively. Moreover, the absence of passivation effects on the Si surface, in the non-aqueous system, ensures that the batteries can maintain their activity and continue to deliver the necessary currents for powering the LED without any significant loss in performance.

Figure 4 presents the performance of the Si-air batteries within the transient electronic device. The voltage and current profiles of the Si-air batteries were recorded during the operation. Figure 4a shows that the average discharge voltage of the alkaline battery remained stable at around 1.1 V while delivering a current density of 0.05 mA cm^{-2}. The LED connected to the battery could be powered for up to 220 h, after which the voltage abruptly dropped to 0.6 V, and the current decreased to values below 0.01 mA cm^{-2}. The status of the LED depending on the time can clearly be seen from the insets in the figure.

During the operation of the device, the passivation of the Si surface was successfully avoided, as the discharge voltage remained above 1 V, and the discharge current densities were below the critical "passivation current" threshold of 0.1 mA cm^{-2}. The specifically designed cell setup, which provided sufficient surface area and enough electrolyte volume, ensured the continued activity of the Si surface until the complete consumption of the active area of the Si anode was achieved. This allowed for extended LED operation without significant performance degradation.

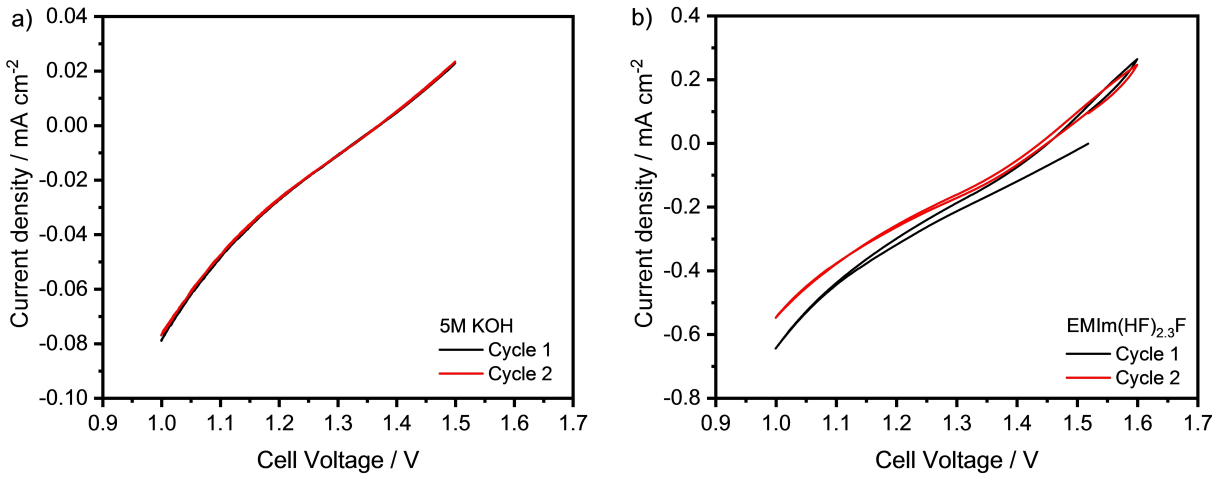

Figure 3. Cyclic voltammograms of a) alkaline Si-air battery, b) non-aqueous Si-air battery in the modified cell setup.

Research Article
doi.org/10.1002/batt.202300573
Chemistry Europe
European Chemical Societies Publishing

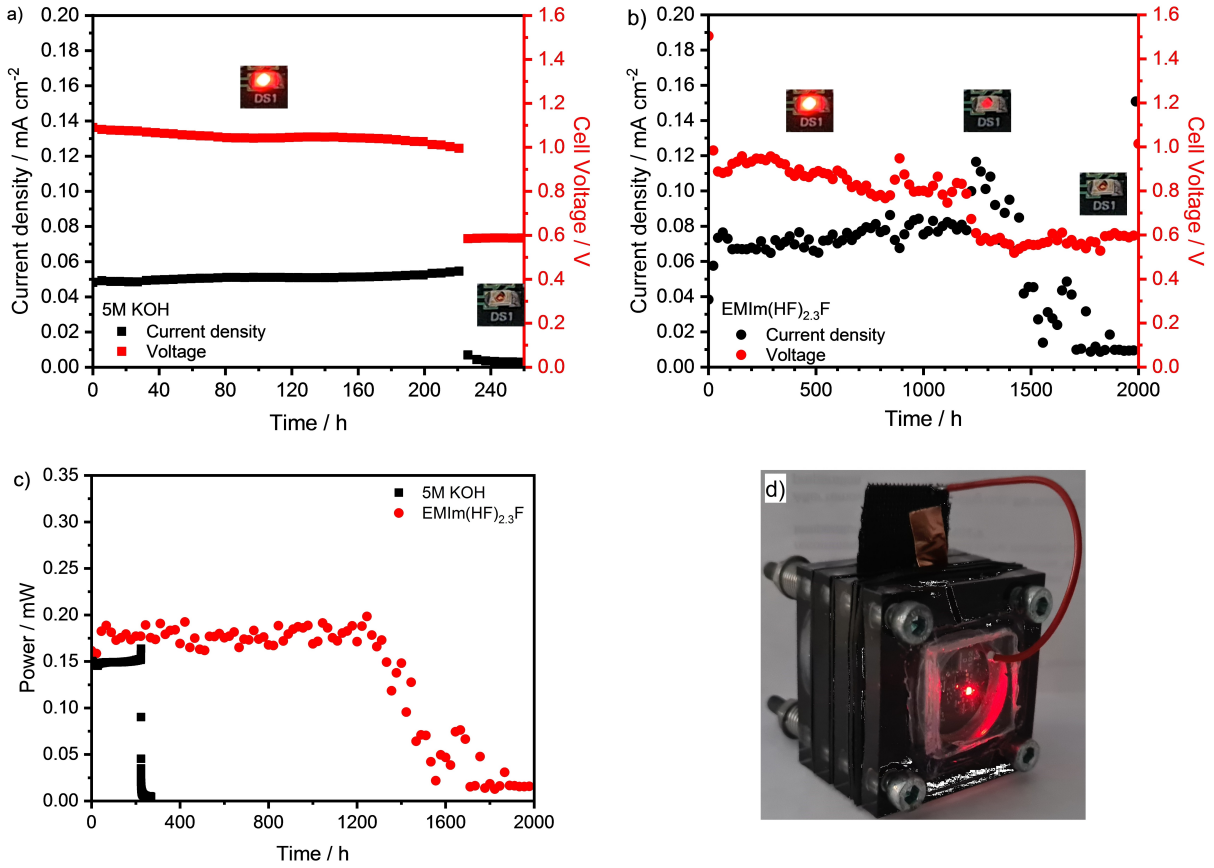

Figure 4. Voltage and current profiles of a) alkaline Si-air battery, b) non-aqueous Si-air battery within the transient electronic device while powering an LED. c) The power output of the both batteries, d) photo of an operating device.

Figure 4b illustrates the voltage/current profiles of the non-aqueous Si-air batteries. Unlike the alkaline battery, the voltage is not as constant as it initiates at 1.5 V and gradually decreases to 1 V within the first 20 h. Subsequently, the voltage drop continues less abruptly, settling around 0.8 V over 1200 h. As previously discussed in Figure 2b, such gradual voltage decay over time is expected. After 1200 h, the battery voltage stabilizes at approximately 0.6 V until the Si anode is fully depleted at around 2000 h. Concurrently, the current density drain of the battery fluctuates between 0.06 and 0.09 mA cm^{-2} during the initial 1200 h. However, due to the abrupt voltage decrease to 0.6 V around 1200 h, the current density increases accordingly to values up to 0.125 mA cm^{-2} to maintain a constant power output. Eventually, the current declines to values close to 0.01 mA cm^{-2} at the end of the discharge.

In the non-aqueous battery, the continuous gradual decay of the voltage over time is closely linked to the chemical and electrochemical reactions occurring at the electrodes during the discharge process. Similar to the reactions suggested for the other metals like Al[37] and Ti,[36] the active anionic specie for Si in the same ionic liquid is $(HF)_2F^-$.[10]

During the battery operation, the oxidation reaction of Si and potential parasitic side corrosion reaction gradually deplete the active anionic species. The Fourier transform infrared (FTIR) characterization of the used electrolytes from discharge experiments in non-aqueous Al-air and Ti-air batteries confirms the depletion of the same active specie.[36,37] The resulting reaction products predominantly remain in the electrolyte, leading to a significant increase in viscosity. As the discharge progresses, this increase in viscosity may contribute to the gradual decrease of the discharge voltage, as observed in Figures 2b and 4b, originating from the sluggish electrochemical reactions and limited mobility of the ionic species.

Figure 4c presents the power output of both alkaline and non-aqueous batteries. The alkaline battery exhibits an average power output of 0.15 mW over a duration of 220 h, while the non-aqueous battery yields a slightly higher average power output of 0.17 mW. The difference in the power output between the batteries is minimal and may have a negligible impact on the brightness of the LED. For reference, the image of the battery while in operation is provided in Figure 4d.

Table 1 provides a summary of the battery performance values for the alkaline and non-aqueous Si-air batteries. The alkaline battery demonstrates a practical specific capacity of 117.2 mAh g_{Si}^{-1}, along with a specific energy of approximately 123.5 Wh kg_{Si}^{-1}. The anode mas conversion efficiency is calculated as 3.06 %, which is in good agreement with the previous literature.[14] In contrast, the non-aqueous Si-air battery exhibits significantly higher performance values. Specifically, the specific capacity and energy of 1072 mAh g_{Si}^{-1} and 841 Wh kg_{Si}^{-1} have

Research Article
doi.org/10.1002/batt.202300573
Chemistry Europe
European Chemical Societies Publishing

Table 1. Performance parameters of the alkaline and non-aqueous Si-air batteries.

	Anode mass conversion efficiency/%	Corrosion rate/mg day^{-1} cm^{-2}	Specific capacity/mAh g_{Si}^{-1}	Specific energy/Wh kg_{Si}^{-1}
KOH	3.06	8.64	117.20	123.58
$EMIm(HF)_{2.3}F$	28.07	1.39	1072.43	841.48

been achieved, respectively. Additionally, the anode mass conversion efficiency is obtained as 28%. The major reason behind the discrepancy in performance between the two batteries can be attributed to the different corrosion rates of Si in the two media. The non-aqueous environment appears to provide more favorable conditions for the battery, resulting in improved overall performance.

Figure 5 demonstrates status of the PCBs before and after the discharge experiments. In Figure 5a, the PCB's initial state is shown before exposure to the electrolytes, where all circuit components and the conduction paths are clearly visible. When the PCB was in contact with 5 M KOH and $EMIm(HF)_{2.3}F$ upon the depletion of the Si anode from discharge experiments in Figure 4, there was a visible corrosion causing detachment of a few components, as shown in Figures 5b and c. Nevertheless, the weight loss of the PCB itself was negligible. A subsequent test with an external power source failed to light the LEDs, probably due to the corroded and damaged components. The information stored in the EEPROM was still accessible even after long exposures to the alkaline and non-aqueous electrolytes. The casing of the EEPROM is made of FR-4, a glass reinforced material based on epoxy laminates that is chemically resistant. In an additional attempt, the EEPROM was decapsulated prior to the experiment, partially exposing the Si die inside within the EEPROM. Figure 5d depicts the corroded Si die within the EEPROM after extended exposure to the alkaline media. Accordingly, the information stored initially was lost due to the damage of the die. Thus, depending on the intended application at remote locations, such a feature might be of interest in order to erase the information within the device.

In summary, this study highlights the potential practical application of Si-air batteries within transient electronics field. The drawbacks of metal-air batteries, particularly their low discharge voltages to power electronics, can be effectively overcome by using DC/DC converters. This allows a single cell to deliver the required power for the intended application. Furthermore, the performance of the Si-air batteries can be further enhanced by modifying the electrolyte through the addition of electrolyte additives or adjusting concentrations, particularly in the alkaline system. Additionally, an alternative approach to improve the design involves placing circuit components directly on the Si backside, thus eliminating the need for PCBs. Due to the semiconductor nature of silicon, micro-electromechanical systems (MEMS) could be directly placed on the back side of the anode and powered by the Si-air battery. Although the complete components of the current

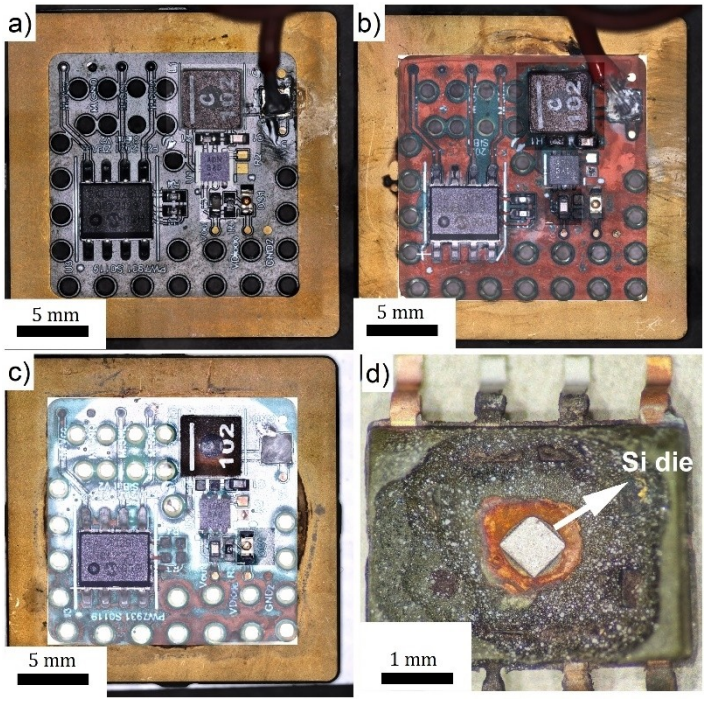

Figure 5. LSM images of the prepared PCBs a) before the experiments, b) after exposure to alkaline media, c) after exposure to non-aqueous media. d) The corroded Si die within the EEPROM after exposure to alkaline media.

system are not fully degradable, further developments could improve the system for still more effective use in applications such as data-secure hardware systems.

Conclusions

This study introduces for the first time the feasibility of utilizing alkaline and non-aqueous Si-air batteries to power vanishing low-power transient electronics, with the intention to allow partial self-destruction of the integrated devices.

Initially, the electrochemical behavior of Si was investigated in standard cells containing 5 M KOH and $EMIm(HF)_{2.3}F$ electrolytes. The activity of the Si anode in both electrolytes were studied by OCV and potentiodynamic polarization experiments, providing crucial insights into the applicable current densities for the electronic circuit designs. The short-term galvanostatic discharge experiments demonstrated that the Si-air battery could be operated effectively under various current densities in both electrolytes without passivation concerns.

The integration of the PCB with the Si-air batteries was initially evaluated in modified cells using cyclic voltammetry experiments to ensure safe operation limits in terms of current and voltage. As a proof of concept for a practical vanishing application, a LED was successfully powered during the battery operation, remaining lit for at least 220 h in the alkaline battery and over 1600 h in the non-aqueous battery. The Si-air batteries exhibit practical specific capacities and energies of 117 $mAh\,g_{Si}^{-1}$ and 123 $Wh\,kg_{Si}^{-1}$ for the alkaline system and 1072 $mAh\,g_{Si}^{-1}$ and 841 $Wh\,kg_{Si}^{-1}$ for the non-aqueous system until the complete consumption of the active area of the Si anodes. Upon assessing the condition of the circuit components after the experiments, it was observed that a few components were corroded and etched away. Subsequent experiments with a decapsulated EEPROM confirmed that the stored information was erased, due to the self-consumption of the Si die by the electrolyte. This particular feature might be of interest for low-power transient electronics, especially applications located in remote areas.

Experimental Section

Material Preparation and Chemicals

Wafers of single crystalline Si doped with As $<100>$ (0.001–0.007 Ω cm) were acquired from University Wafer and cut into 11×11 and 24×24 mm^2 square pieces. The Si wafers were treated by a two-step plasma process (PICO, Diener) prior to the experiments. The first step consisted of removal of organic contamination by Ar/O_2 plasma while the second step involved Ar/SF_6 to remove any oxide layer on the Si wafers. The freshly treated wafers were kept in an Ar atmosphere and directly used for the assembling of the battery. KOH pellets (≥85% KOH basis, Sigma-Aldrich) and deionized water (PURELAB Elga, conductivity ≥0.1 $\mu S\,cm^{-1}$) were used for the preparation of 5 M KOH electrolyte. The KOH solutions were purged with Ar to reduce the dissolved oxygen. The $EMIm(HF)_{2.3}F$ ionic liquid was acquired from Morita Chemical Industries and was directly employed as electrolyte. The mass of the silicon anodes was measured by an analytical balance with an accuracy of ±0.01 mg (XA205, Mettler Toledo). The carbon-based air cathodes with manganese oxide catalyst (E4 type) were purchased from Electric Fuel Ltd.

Electrochemical measurements

Standard Si-air battery: All the electrochemical experiments were performed in a cell setup made from Poly(methyl methacrylate). The schematic of the cell setup is shown in Figure S4. The non-aqueous cell setup was adapted from Cohn et al.[6] The alkaline cell setup was a refill-type that was introduced previously.[14] The half-cell consisted of a three-electrode setup with Si as working, Pt as counter, and a ferrocene/ferrocenium-based gel electrode or a commercial mercury/mercury oxide as reference electrodes. The reference electrode was prepared according to Shvartsev et al.[41] The full-cell setup consisted of a Si wafer as anode, commercial carbon-based air electrodes as cathode, and either $EMIm(HF)_{2.3}F$ or 5 M KOH as electrolyte. The geometrical surface areas of the electrodes were 0.44 cm^2. The electrolyte volume of the cell was 0.6 mL in all experiments.

Vanishing Si-air battery in transient electronics: The experimental setup is composed of three pieces of Poly(methyl methacrylate) (PMMA), as shown in Figure 6a. An optically transparent window was used on the anode side to facilitate real-time monitoring of both the circuit's status and the LED. The geometrical surface areas of the electrodes were 2.8 cm^2, while the electrolyte volume within the cell was 3.0 mL. The cell consisted of a Si wafer with the integrated circuit on the backside as anode, commercial air electrode as cathode, and $EMIm(HF)_{2.3}F$ or 5 M KOH as electrolyte.

Circuit design: The integrated circuit encompasses multiple components, as shown in Figure 6b. The circuit elements and types were carefully selected to enable the powering of a low-power requirement component with a single Si-air battery. For illustrative purposes, a small red LED (TLMS1000-GS08, Mouser Electronics) was employed, which allows visual monitoring during operation. Likewise, further adjustments to both the circuit and the battery may permit the utilization of additional low power requirement components, such as microchips. An EEPROM (24LC02B–I, Mouser Electronics) was also included in the integrated circuit to store information. A DC-DC converter (MAX17220ELT+T, Mouser Electronics) was employed to achieve the necessary voltage matching for the LED operation. The circuit components were placed on the commercially available printed circuit boards (PCBs). The PCB was coupled with the backside of the Si wafer. A detailed description of the integrated circuit components is presented in Table 2.

Characterization methods: Electrochemical experiments were performed by using the Biologic VMP3 potentiostat. Before each standard electrochemical experiment, the cells were allowed to rest for 4 h. The potentiodynamic polarization and cyclic voltammetry experiments were conducted with a scan rate of 5 $mV\,s^{-1}$. Galvanostatic discharge experiments were performed by applying current densities of a) 0.025, 0.05, and 0.07 $mA\,cm^{-2}$ for the alkaline system, and b) 0.05, 0.10, and 0.30 $mA\,cm^{-2}$ for the non-aqueous system. In the case of the battery with an integrated circuit, the current was measured via a zero-resistance ammeter (ZRA) mode of the potentiostat with a parallel channel. All the experiments were conducted in a climate chamber (Binder KMF115) to ensure controlled conditions of 25 °C and 50% relative humidity. The condition of the silicon anodes with mounted circuits prior to and after the experiments were analyzed by using a confocal laser scanning microscope (OLS4100, Olympus Corp., Japan).

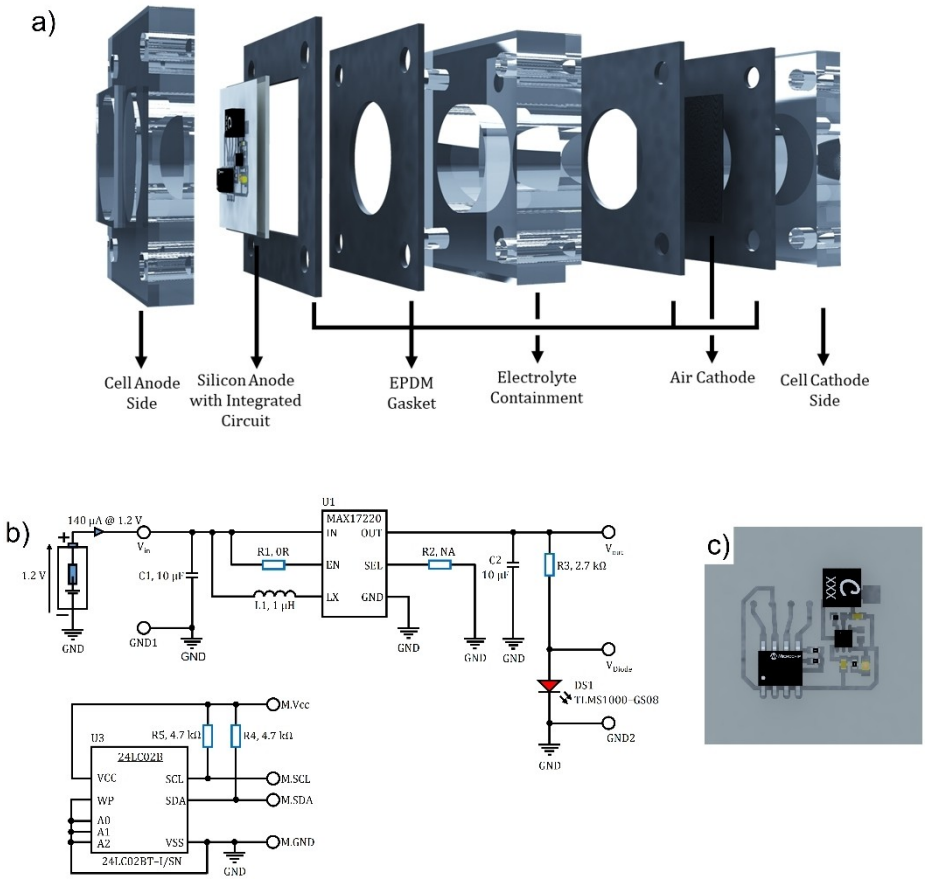

Figure 6. a) The modified cell assembly of the PCB/Si-air battery as a transient electronic device. b) A detailed diagram of the DC/DC converter and the EEPROM, c) 3D representation of the PCB on the backside of silicon anode.

Table 2. List of components for the integrated circuit coupled to the Si-air battery.

Symbol	Description
C1	Capacitor SMD 1005 0402 2–10 µF
C2	Capacitor SMD 1005 0402 2–10 µF
DS1	Low Current LED, 40 mW, 1.8 V, −40 to 100 °C, 2-Pin SMD (0603), RoHS, Tape and Reel
L1	XFL4020-102MEC Shielded Power Inductor, 1 µH, 64 MHz, −40 to 125 °C, 2-Pin SMD, RoHS, Tape and Reel
R1	Resistor SMD 1005 0402 1/16 W
R2	NA = 1.8 V
R3	Resistor SMD 1005 0402 1/16 W
R4	Resistor SMD 1005 0402 1/16 W
R5	Resistor SMD 1005 0402 1/16 W
U1	IC REG BOOST ADJ 225MA 6UDFN
U3	24LC02B-I/SN 256×8–1.8 V

Acknowledgements

This research was funded by the German Federal Ministry of Education and Research (BMBF) within the project Verbundvorhaben iNEW2.0 (03SF0627 A). Technion's researchers were partially funded by Grand Technion Energy program (GTEP), the 2nd Israeli National Research on Electrochemical Propulsion (INREP 2) and by the Israeli National Center for Sustainable Energy (I-NISE). Open Access funding enabled and organized by Projekt DEAL.

Conflict of Interests

The authors declare no conflict of interest.

Data Availability Statement

The data that support the findings of this study are available from the corresponding author upon reasonable request.

Keywords: silicon-air battery · aqueous and non-aqueous electrolyte · self-consumed · vanishing power devices · transient electronics

[1] S. Chen, M. Zhang, P. Zou, B. Sun, S. Tao, *Energy Environ. Sci.* **2022**, 1805.
[2] I. Hasa, P. Adelhelm, G. Cao, L. Mai, *Batteries & Supercaps* **2021**, *4*, 1036.
[3] Q. Liu, Z. Pan, E. Wang, L. An, G. Sun, *Energy Storage Mater.* **2020**, *27*, 478.
[4] H. Weinrich, Y. E. Durmus, H. Tempel, H. Kungl, R.-A. Eichel, *Materials (Basel).* **2019**, *12*, 2134.
[5] G. Cohn, D. Starosvetsky, R. Hagiwara, D. D. Macdonald, Y. Ein-Eli, *Electrochem. Commun.* **2009**, *11*, 1916.

[6] G. Cohn, Y. Ein-Eli, *J. Power Sources* **2010**, *195*, 4963.
[7] G. Cohn, D. D. Macdonald, Y. Ein-Eli, *ChemSusChem* **2011**, *4*, 1124.
[8] P. Jakes, G. Cohn, Y. Ein-Eli, F. Scheiba, H. Ehrenberg, R.-A. Eichel, *ChemSusChem* **2012**, *5*, 2278.
[9] G. Cohn, R.-A. Eichel, Y. Ein-Eli, *Phys. Chem. Chem. Phys.* **2013**, *15*, 3256.
[10] Y. E. Durmus, S. Jakobi, T. Beuse, Ö. Aslanbas, H. Tempel, F. Hausen, L. G. J. de Haart, Y. Ein-Eli, R.-A. Eichel, H. Kungl, *J. Electrochem. Soc.* **2017**, *164*, A2310.
[11] Y. E. Durmus, C. Roitzheim, H. Tempel, F. Hausen, Y. Ein-Eli, H. Kungl, R.-A. Eichel, *J. Appl. Electrochem.* **2020**, *50*, 93.
[12] X. Zhong, H. Zhang, Y. Liu, J. Bai, L. Liao, Y. Huang, X. Duan, *ChemSusChem* **2012**, *5*, 177.
[13] D. W. Park, S. Kim, J. D. Ocon, G. H. A. Abrenica, J. K. Lee, J. Lee, *ACS Appl. Mater. Interfaces* **2015**, *7*, 3126.
[14] Y. E. Durmus, Ö. Aslanbas, S. Kayser, H. Tempel, F. Hausen, L. G. J. de Haart, J. Granwehr, Y. Ein-Eli, R.-A. Eichel, H. Kungl, *Electrochim. Acta* **2017**, *225*, 215.
[15] R. Schalinski, S. L. Schweizer, R. B. Wehrspohn, *ChemSusChem* **2023**, *16*, e202300077.
[16] O. J. Glembocki, R. E. Stahlbush, M. Tomkiewicz, *J. Electrochem. Soc.* **1985**, *132*, 145.
[17] E. D. Palik, O. J. Glembocki, J. D. Rinko, I. Heard, *J. Electrochem. Soc.* **1989**, *136*, 1420.
[18] H. Seidel, L. Csepregi, A. Heuberger, H. Baumgartel, *J. Electrochem. Soc.* **1990**, *137*, 3612.
[19] P. Allongue, V. Costa-Kieling, H. Gerischer, *J. Electrochem. Soc.* **1993**, *140*, 1009.
[20] Y. E. Durmus, S. S. Montiel Guerrero, Ö. Aslanbas, H. Tempel, F. Hausen, L. G. J. de Haart, Y. Ein-Eli, R.-A. Eichel, H. Kungl, *Electrochim. Acta* **2018**, *265*, 292.
[21] D. Chen, X. Zhang, Y. Zhang, Z. Liu, F. Deng, Y. Yu, *Surf. Interfaces* **2023**, *38*, 102777.
[22] R. Schalinski, P. Mörstedt, S. L. Schweizer, R. B. Wehrspohn, *Adv. Energy Sustain. Res.* **2023**, 2300138.
[23] L. A. Wehner, N. Mittal, T. Liu, M. Niederberger, *ACS Cent. Sci.* **2021**, *7*, 231.
[24] N. Mittal, A. Ojanguren, M. Niederberger, E. Lizundia, *Adv. Sci.* **2021**, *8*, 1.
[25] S. Hwang, S. Kang, X. Huang, M. A. Brenckle, F. G. Omenetto, J. A. Rogers, *Adv. Mater.* **2015**, *27*, 47.
[26] R. Jamshidi, M. Taghavimehr, Y. Chen, N. Hashemi, R. Montazami, *Adv. Sustainable Syst.* **2022**, *6*, 1.
[27] Y. Chen, H. Wang, Y. Zhang, R. Li, C. Chen, H. Zhang, S. Tang, S. Liu, X. Chen, H. Wu, R. Lv, X. Sheng, P. Zhang, S. Wang, L. Yin, *Nanotechnology* **2019**, *30*, 394002.
[28] C. H. Lee, J. W. Jeong, Y. Liu, Y. Zhang, Y. Shi, S. K. Kang, J. Kim, J. S. Kim, N. Y. Lee, B. H. Kim, K. I. Jang, L. Yin, M. K. Kim, A. Banks, U. Paik, Y. Huang, J. A. Rogers, *Adv. Funct. Mater.* **2015**, *25*, 1338.
[29] S. Pandey, C. Mastrangelo, *Micromachines* **2022**, *13*, 242.
[30] S. S. Pandey, N. Banerjee, Y. Xie, C. H. Mastrangelo, *Adv. Mater. Technol.* **2018**, *3*, 1.
[31] S. Liu, X. Wang, S. Liu, Y. Deng, B. Zhao, H. Wang, X. Sheng, L. Zhao, L. Wang, P. Zhang, L. Yin, *Adv. Eng. Mater.* **2023**, *25*, 2300213.
[32] R. W. Revie, *Uhlig's Corrosion Handbook*, Third., John Wiley and Sons, **2011**.
[33] P. Allongue, V. Costa-Kieling, H. Gerischer, *J. Electrochem. Soc.* **1993**, *140*, 1018.
[34] R. M. Hurd, N. Hackerman, *Electrochim. Acta* **1964**, *9*, 1633.
[35] S. Cattarin, M. M. Musiani, *J. Phys. Chem. B* **1999**, *103*, 3162.
[36] Y. E. Durmus, M. Kaltenberg, K. Dzieciol, M. Schalenbach, D. Gelman, B. Shvartsev, H. Tempel, H. Kungl, R. A. Eichel, Y. Ein-Eli, *Chem. Eng. J.* **2023**, *461*, 141903.
[37] D. Gelman, B. Shvartsev, I. Wallwater, S. Kozokaro, V. Fidelsky, A. Sagy, A. Oz, S. Baltianski, Y. Tsur, Y. Ein-Eli, *J. Power Sources* **2017**, *364*, 110.
[38] N. R. Levy, M. Auinat, Y. Ein-Eli, *Energy Storage Mater.* **2018**, *15*, 465.
[39] E. D. Palik, O. J. Glembocki, I. Heard, *J. Electrochem. Soc.* **1987**, *134*, 404.
[40] E. D. Palik, O. J. Glembocki, I. Heard, P. S. Burno, L. Tenerz, *J. Appl. Phys.* **1991**, *70*, 3291.
[41] B. Shvartsev, G. Cohn, H. Shasha, R.-A. Eichel, Y. Ein-Eli, *Phys. Chem. Chem. Phys.* **2013**, *15*, 17837.

Manuscript received: January 8, 2024
Revised manuscript received: January 16, 2024
Version of record online: January 29, 2024